Supplementary Information: Microscale resolution thermal mapping using a flexible platform of patterned quantum sensors

Paolo Andrich,[†,¶] Jiajing Li,[†,¶] Xiaoying Liu,[†] F. Joseph Heremans,[‡,†] Paul F. Nealey,[†,‡] and David D. Awschalom[*,†,‡]

†*Institute for Molecular Engineering, Chicago, IL 60637, USA*

‡*Institute for Molecular Engineering and Materials Science Division, Argonne, IL 60439, USA*

¶*These two authors contributed equally*

E-mail: awsch@uchicago.edu

Supplementary Notes

Notes on the COMSOL simulation

To simulate the temperature distribution generated by the coplanar waveguide (CPW) shown in Fig. 4b of the main text we use the Electric Currents, Shell and the Heat Transfer physics COMSOL Multiphysics® modules coupled through the Boundary Electromagnetic Heat Source Multiphysics module. The nominal design used to lithographically pattern the device on the Gadolinium Gallium Garnet (GGG) substrate is also used to simulate the microwave antenna (see Figure S4). To simplify the model we consider the CPW as comprised of a single 200 nm thick gold layer. The CPW used in the experiment also include a 6 nm thick titanium adhesion layer between the GGG substrate and the gold.

In the following we report the details of the model's geometry and the parameters for the thermal properties of the materials:

- Copper plate:
  - $2.5 \times 2.5 \times 0.5\,\mathrm{mm}$
  - Thermal conductivity: $385\,\mathrm{W/m \cdot K}$
  - Heat capacity at constant pressure: $385\,\mathrm{J/kg \cdot K}$
- Gadolinium Gallium Garnet substrate:
  - $2.5 \times 2.5 \times 0.5\,\mathrm{mm}$
  - Thermal conductivity: $7.05\,\mathrm{W/m \cdot K}$
  - Heat capacity at constant pressure: $381.2\,\mathrm{J/kg \cdot K}$
- Gold:
  - Thermal conductivity: $314\,\mathrm{W/m \cdot K}$
  - Heat capacity at constant pressure: $129\,\mathrm{J/kg \cdot K}$
- PDMS:
  - $2.4 \times 0.8 \times 0.1\,\mathrm{mm}$
  - Thermal conductivity: $0.15\,\mathrm{W/m \cdot K}$
  - Heat capacity at constant pressure: $1460\,\mathrm{J/kg \cdot K}$
- Heat transfer at the GGG-air and PDMS-air interface: $5\,\mathrm{W/m^2 \cdot K}$
- Heat transfer at the copper heat-sink surface. Due to the complexity in fully modeling the sample holder and the complete setup we use this as a free parameter to allow for the emergence of the same range of temperatures observed in the experimental data. Through this process we obtain $300\,\mathrm{W/m^2 \cdot K}$.

Additional Temperature Measurements

To support the validity of our conclusions and of the assumptions made in the model describing the heat dissipation of the sample, we collect additional temperature measurements from particles belonging to the same array shown in Figure 3(a) and used to obtain the data in Figure 4(a). In particular, we placed this array on two additional substrates in the proximity of microwave striplines (see Figure S5a) and measure the temperature generated by a continuous current driven through these antennas. We select particles containing NV centers closely aligned with the magnetic field generated by the antenna to more easily extract the value of the zero-field splitting from the data.[1] In Figure S5b, we report the data collected on a GGG substrate for different values of the applied current using one ND of the array located $17\,\mu\mathrm{m}$ from the stripline. The orange line shows the calculated values of the temperature as extracted from a COMSOL Multiphysics® simulation in which we use the same parameters employed in Figure 4(b). The rather large error bars are due to the small contrast shown by this particle, which is in part due to the fact that we cannot apply stronger microwave signals without introducing additional heating in the system. Figure S8c shows an analogous set of data collected on a particle positioned on a yttrium iron garnet (YIG) substrate, $13\,\mu\mathrm{m}$ from the stripline. Taking advantage of the enhanced spin wave mediated interactions between the microwave fields and the NV centers' spin,[2] we can obtain a larger signal-to-noise ratio even with very small microwave input powers. On the other side, the measurements on YIG are complicated by the possibility of seeing only one of the NV center's spin transitions. In this case, to discriminate between the magnetic field and temperature effects on the resonance position we extract the components of the resonance shift that are linear (magnetic field effect) and quadratic (heating effect) in the applied current. The orange line again indicates the simulated temperature values, obtained here by only changing the GGG material parameters with the YIG ones. These results demonstrate the reusability of the ND arrays and are a confirmation of their accuracy as temperature sensors.

We note that we have used the same sensing device for further tests and we have not seen any degradation of the quality of the arrays after ~ 10 repeated uses, as long as they are kept clean and not exposed to solvents that can induce swelling of the PDMS matrix.

Supplementary Figures

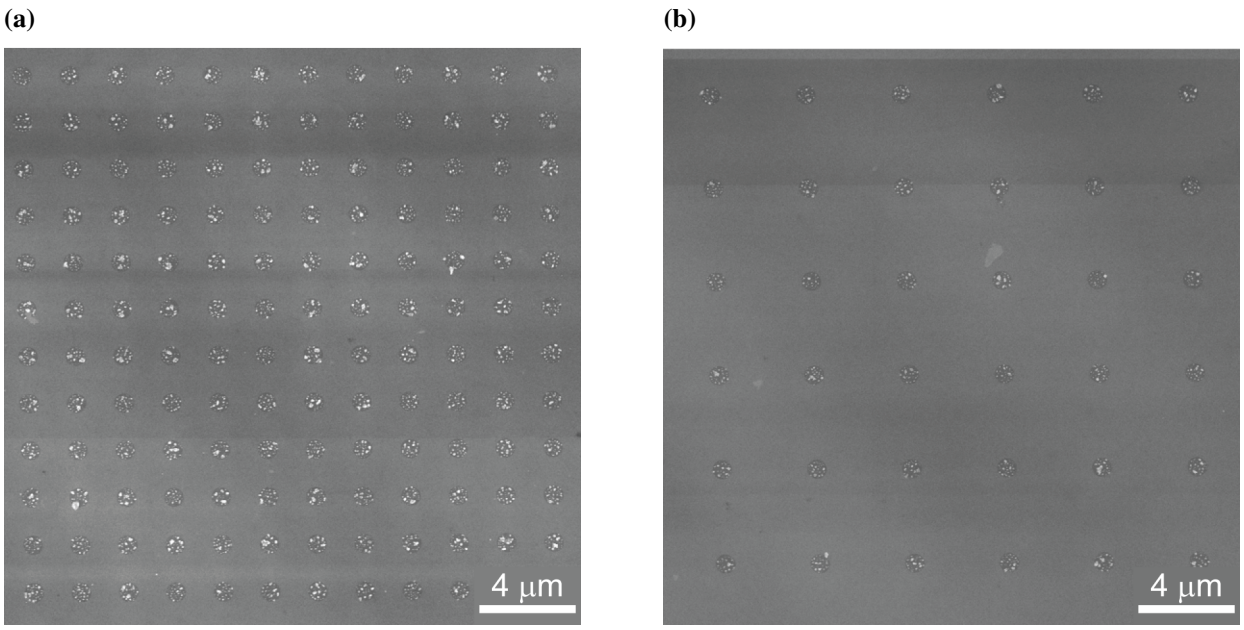

Figure S1: SEM images of two arrays of patterned $1000\,\mathrm{nm}$ circles with (a) 2 and (b) $4\,\mu\mathrm{m}$ pitch. No significant differences in the array coverage were observed while changing the distance between the patterned regions.

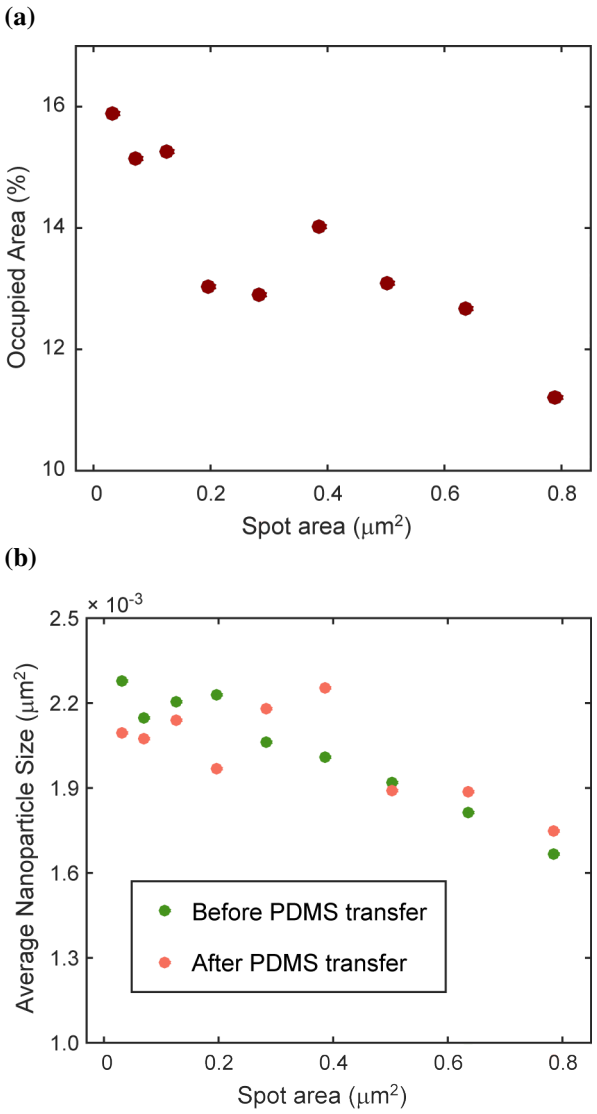

Figure S2: (a) Percentage of the patterned areas occupied by the diamond nanoparticles as a function of the circle size. The nanodiamonds' (NDs) density decreases with increasing patterned area size, which could be associated with a higher transfer efficiency of the particles to the PDMS matrix. The data point for the smallest spot size ($100\,\mathrm{nm}$) is not reported in this figure. The percentage of occupied area is in this case significantly higher ($\sim 24\,\%$ on average) but, as the spot size is comparable with the average ND size and the average number of NDs per spot is smaller than one, this value is not indicative of the nanoparticle density. (b) Average size of the nanoparticles residing on a the silicon substrate before and after the PDMS transfer step as a function of the patterned spot area. This data is obtained by analyzing SEM images of patterned spots (see for instance Fig.1 of the main text) with the ImageJ software. As no significant difference is observed, we conclude that the NDs' transfer efficiency into the PDMS matrix is independent of their size.

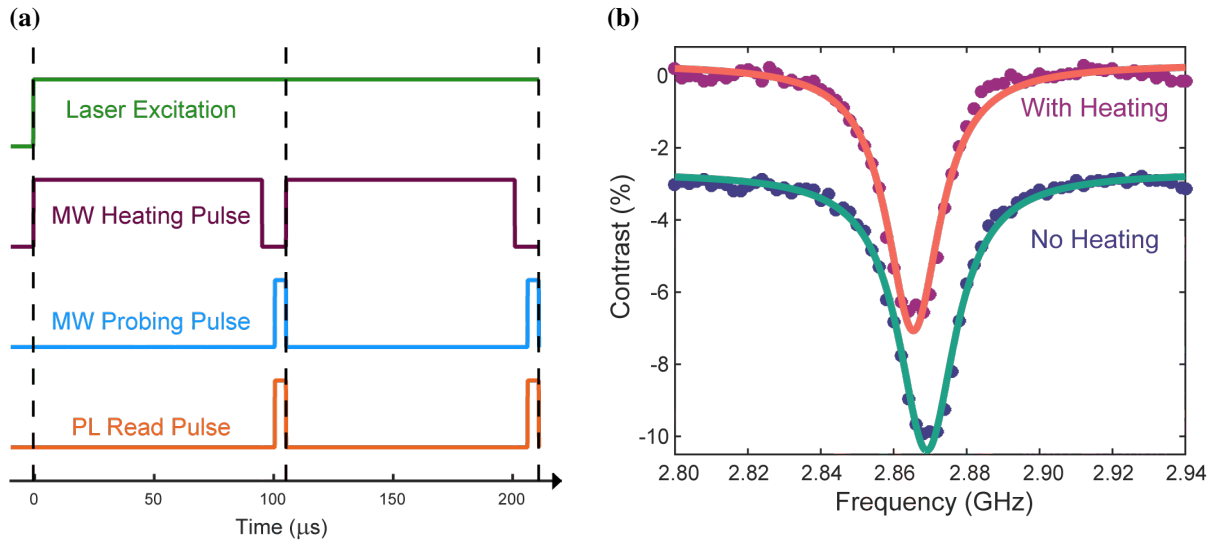

Figure S3: (a) Pulse sequence used to collect the ODMR spectra in the presence of a microwave heating pulse. The $532\,\mathrm{nm}$ excitation laser is always present, while the microwave signal is switched between a $100\,\mu\mathrm{s}$, $0.4\,\mathrm{W}$ off-resonant heating pulse and a $5\,\mu\mathrm{s}$, $3.5\,\mathrm{mW}$ pulse of varying frequency used to probe the NV centers' resonance. The photoluminescence signal is collected during the course of the microwave probing pulse by gating a data acquisition module. A short $500\,\mathrm{ns}$ delay separates the two microwave pulses to avoid spurious driving of the NV centers' spin during the acquisition time. Two periods of the pulse sequence are shown for clarity. (b) Example of typical ODMR spectra collected at zero magnetic field in the presence and absence of the heating pulse. The temperature change at the NV center's location is inferred from the shift in the ODMR resonance frequency.

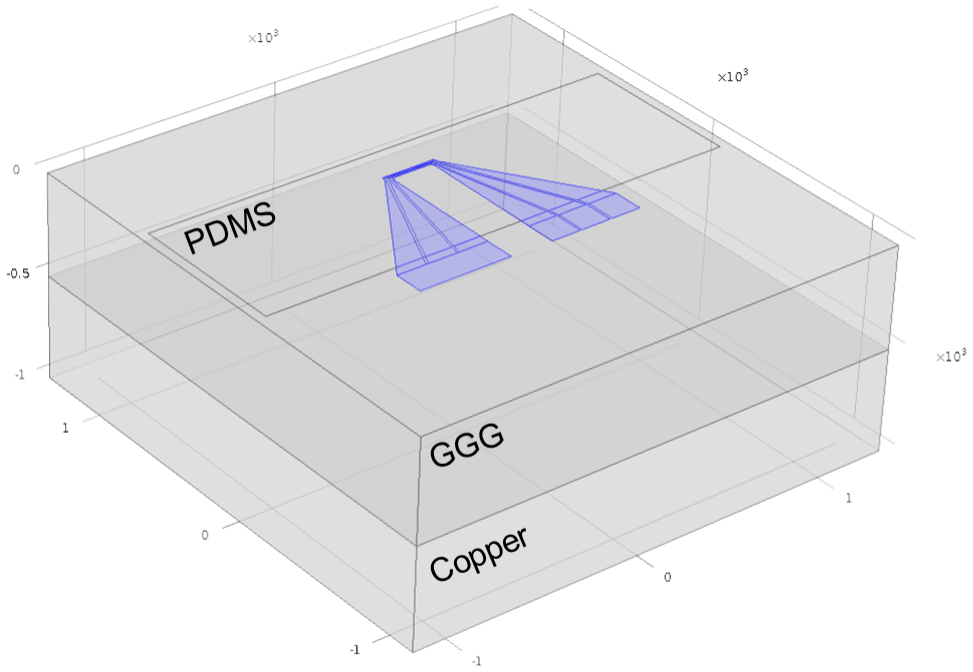

Figure S4: Design of the COMSOL Multiphysics® model. The bottom layer represents the copper heat-sink, above which the Gadolinium Gallium Garnet substrate resides. The coplanar waveguide (represented in the model as a shell conductor of $200\,\mathrm{nm}$ thickness) is highlighted. The layout of the PDMS layer is visible in the region of the antenna.

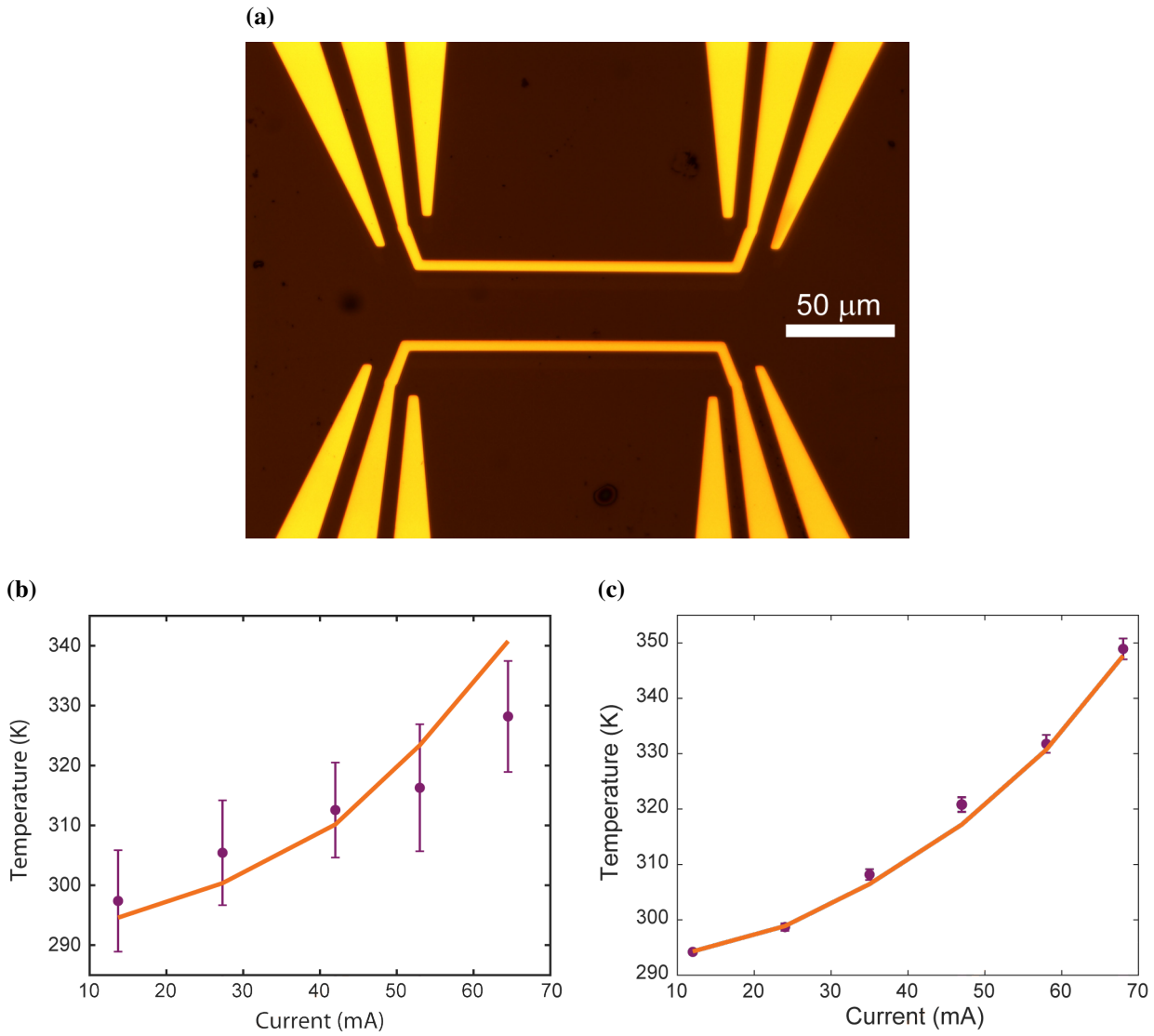

Figure S5: (a) Optical image of a pair of micro stripline antennas used to control the NV center spin and introduce temperature variations through Joule heating induced by a DC current. (b) The data points correspond to the temperature detected with a ND 17 µm away from a stripline antenna patterned on a GGG substrate as a function of the applied DC current. The orange line is the calculated temperature as obtained with the same model used in the main text (see Figure 4(b)). (c) Analogous set of data obtained with a ND placed 13 µm away from an antenna patterned on a YIG substrate. The calculated temperature is again extracted from the same model where only the GGG material parameters were replaced with the YIG ones.

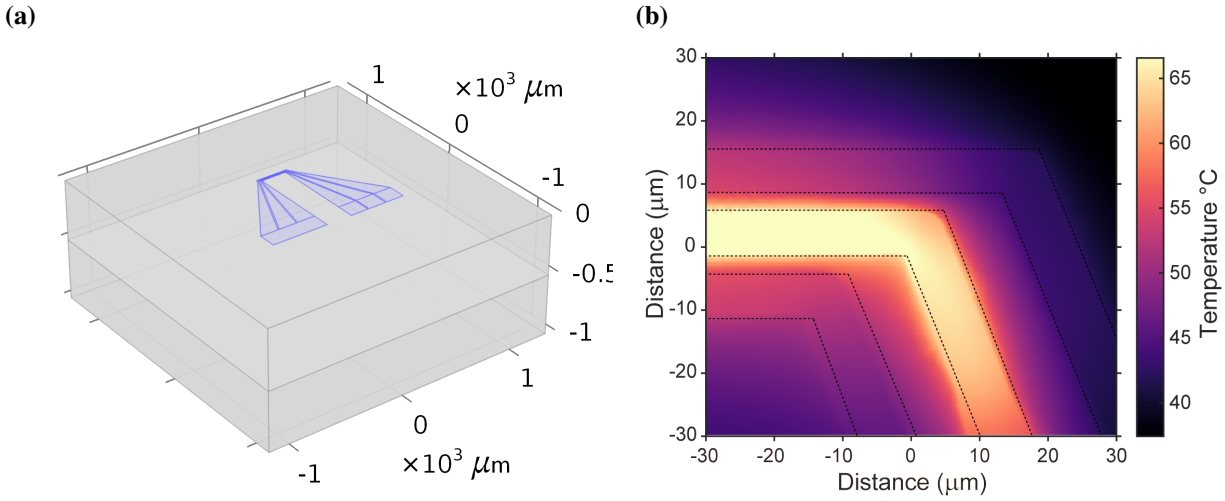

Figure S6: (a) Geometry of the COMSOL Multiphysics® model without the PDMS layer. (b) Simulated temperature map of the region of the microwave antenna investigated in the main text in the absence of the PDMS layer. This map closely mirror the one shown in Fig. 4b, which describes the system complete of the PDMS matrix. This supports the assumption that the PDMS layer does not introduce relevant spurious thermal dissipation channels in the system.

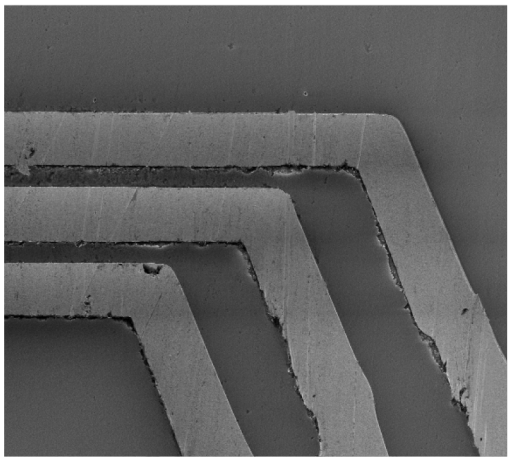

Figure S7: Scanning electron microscopy image of the region of the microwave antenna that was thermally imaged in this work. Imperfections in the antenna geometry are clearly visible.

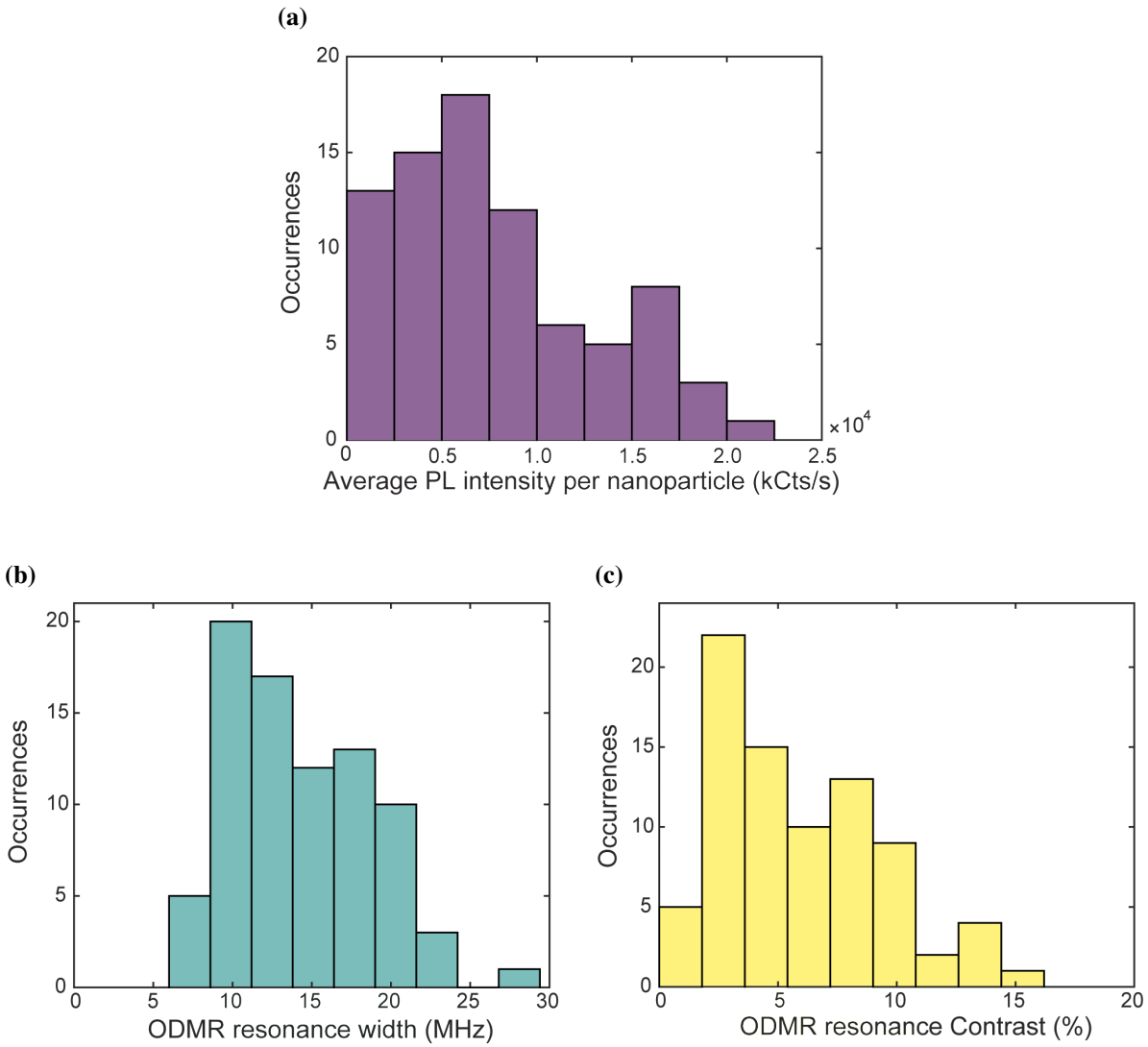

Figure S8: Statistics on the photoluminescence and ODMR resonance properties collected on the 81 measured nanodiamonds. (a) Photoluminescence averaged across the ODMR spectrum. (b) ODMR resonance width. (c) Contrast of the ODMR resonance.

References

(1) Tetienne, J. P.; Rondin, L.; Spinicelli, P.; Chipaux, M.; Debuisschert, T.; Roch, J.-F.; Jacques, V. *New Journal of Physics* **2012**, *14*, 103033.

(2) Andrich, P.; de las Casas, C. F.; X., L.; Bretscher, H. L.; Berman, J. R.; Heremans, F. J.; Nealey, P. F.; Awschalom, D. D. *npj Quantum Info.* **2017**, *3*, 28.